Available online at www.sciencedirect.com
ScienceDirect
Trans. Nonferrous Met. Soc. China 20(2010) 1892−1898
Transactions of Nonferrous Metals Society of China
www.tnmsc.cn

Effects of Na content on structure and electrochemical performances of $Na_xMnO_{2+\delta}$ cathode material

YANG Shun-yi(杨顺毅)[1], WANG Xian-you(王先友)[1], WANG Ying(王 莹)[2],
CHEN Quan-qi(陈权启)[1], LI Jiao-jiao(李姣姣)[1], YANG Xiu-kang(杨秀康)[1]

1. Key Laboratory of Environmentally Friendly Chemistry and Applications of Ministry of Education, School of Chemistry, Xiangtan University, Xiangtan 411105, China;
2. School of Chemical Engineering and Pharmacy, Wuhan Institute of Technology, Wuhan 430073, China

Received 10 September 2009; accepted 2 February 2010

Abstract: Sodium manganese oxides, $Na_xMnO_{2+\delta}$ (x = 0.4, 0.5, 0.6, 0.7, 1.0; δ = 0−0.3), were synthesized by solid-state reaction routine combined with sol-gel process. The structure, morphology and electrochemical performances of as-prepared samples were characterized by XRD, SEM, CV, EIS and galvanostatic charge/discharge experiments. It is found that $Na_{0.6}MnO_{2+\delta}$ and $Na_{0.7}MnO_{2+\delta}$ have high discharge capacity and good cycle performance. At a current density of 25 mA/g at the cutoff voltage of 2.0−4.3 V, $Na_{0.6}MnO_{2+\delta}$ gives the second discharge capacity of 188 mA·h/g and remains 77.9% of second discharge capacity after 40 cycles. $Na_{0.7}MnO_{2+\delta}$ exhibits the second discharge capacity of 176 mA·h/g and shows better cyclic stability; the capacity retention after 40 cycles is close to 85.5%. Even when the current density increases to 250 mA/g, the discharge capacity of $Na_{0.7}MnO_{2+\delta}$ still approaches to 107 mA·h/g after 40 cycles.
Key words: lithium-ion battery; cathode material; sodium manganese oxides; electrochemical properties; sol-gel technology

1 Introduction

Manganese oxides have generated a great deal of interest as a kind of cathode material for rechargeable lithium batteries due to their high specific energy, low cost, low toxicity and safe performance[1]. Many works have been studied on the synthesis and characterization of kinds of electrochemically active manganese oxides based on the Li-Mn-O system. However, some problems still exist in the utilization of lithium manganese oxides as cathode in the practical Li-ion batteries[2].

In recent years, other kinds of electrochemically active manganese oxides based on Na-Mn-O system[3−4] have been concerned. $Na_{0.45}MnO_{2.14}\cdot 0.76H_2O$ with interlayer water prepared by a sol-gel process involving the reduction of sodium permanganate by reductive organic agents such as the fumaric acid was reported by GOFF et al[5]. Its stable capacity was about 130 mA·h/g on extended cycling at *C*/6 rate in the potential range of 2.0−4.2 V. However, the rate capability was found to be rather low due to the presence of interlayer water. HIBINO et al[6] prepared composite material of hydrated manganese oxide with acetylene black and evaluated the material availability as a lithium battery cathode. The results show a discharge capacity of 340 mA·h/g at a rate of 10 mA/g and 233 mA·h/g even at a large discharge current of 10 000 mA/g. This rapid discharge was possibly caused by the structure of the composite in which the constituents were small enough and highly dispersed and had favorable contact conditions. But, it also shows a poor cyclic stability where only half of the first discharge capacity is remained after the 5th cycle, and this is also probable due to the presence of interlayer water. Recently, the anhydrous sodium manganese oxide α-$Na_{0.66}MnO_{2.13}$ synthesized via a sol-gel process in organic medium using $NaMnO_4$ as manganese source and CH_3OH as reducing agent was reported by BACH et al[7], and they stabilized its layer structure by using acetylene black during the synthetic reaction. The cyclic stability of the material was successfully improved, and a stable specific

Foundation item: Project(20871101) supported by the National Natural Science Foundation of China; Project(08A067) supported by Research Foundation of Education Bureau of Hunan Province, China
Corresponding author: WANG Xian-you; Tel: +86-731-58292060; Fax: +86-731-58292061; E-mail: wxianyou@yahoo.com
DOI: 10.1016/S1003-6326(09)60391-5

capacity of 180 mA·h/g was observed at *C*/20 in the cycling limits 2.0−4.3 V with an average working voltage of 3 V without the emergence of spinel phase after 50 cycles. This shows that anhydrous sodium manganese oxide is a stable cathode material for the application of secondary lithium batteries.

The studies mentioned above all used reducing methods to synthesize the sodium manganese oxides. Previous works[8−9] in our group showed that anhydrous $Na_{0.7}MnO_{2+\delta}$ could be prepared by oxidation methods (solid-state reaction routine combining with sol-gel process) using $Mn(CH_3CO_2)_2{\cdot}4H_2O$ as the manganese source. The effects of calcination temperature on the structure and electrochemical performance of the materials were discussed, and it was found that 600 °C is an optimal calcination temperature to prepare an anhydrous hexagonal layer P2 structure compound. In this work, cathode materials $Na_xMnO_{2+\delta}$ (x = 0.4, 0.5, 0.6, 0.7 and 1.0) were prepared using our previous technology and the effects of sodium content on the structure and electrochemical properties of $Na_xMnO_{2+\delta}$ were studied in detail.

2 Experimental

$Na_xMnO_{2+\delta}$ were prepared by mixing Na_2CO_3 (AR, 99%) and $Mn(CH_3CO_2)_2{\cdot}4H_2O$ (AR, 99%) in distilled water at the ratio of n_{Na}/n_{Mn} = 0.4, 0.5, 0.6, 0.7 and 1.0, respectively. After rotary evaporation, the mixtures were heated in air at 250 °C for 12 h to decompose the acetates. The resulting powder was then fired at the temperature of 600 °C in air for 1 h followed by cooling. The samples with different stoichiometric ratios of Na to Mn were obtained. The samples $Na_xMnO_{2+\delta}$ with x of 0.4, 0.5, 0.6, 0.7 and 1.0 were referred as 0.4-SMO (sodium manganese oxide), 0.5-SMO, 0.6-SMO, 0.7-SMO, 1.0-SMO, respectively.

The phase identification of the samples was performed with a diffractometer (D/Max-3C, Rigaku, Japan) using Cu K_α radiation (λ=1.54178 Å) and a graphite monochromator at 36 kV and 20 mA. The scanning rate was 8 (°)/min and the scanning range of diffraction angle (2θ) was $10° \le 2\theta \le 80°$. The surface morphology of the samples was observed using the JSM-5600LV SEM (JEOL, Japan).

The electrochemical tests of $Na_xMnO_{2+\delta}$ samples were carried out using coin cells assembled in an argon-filled glove box. In all cells, the cathode consisted of a mixture of active material (70%), acetylene black (20%), graphite (5%) and polyvinylidene fluoride (PVDF) as binder agent (5%), lithium served as counter and reference electrodes. A Celgard 2400 was used as a separator, and the electrolyte was a 1 mol/L $LiPF_6$ solution in ethylene carbonate (EC)-dimethyl carbonate (DMC) (1:1, volume ratio). Galvanostatic discharge−charge measurements were carried out in Neware battery test system BTS-XWJ-6.44S-00052 (Newell, Shenzhen, China) at a current density of 25, 50, 125, 250 mA/g between 2.0 and 4.3 V vs Li/Li^+ at room temperature. Cyclic voltammogram (CV) was measured at a scan rate of 50 μV/s between 2.0 and 4.3 V using a CHI600A electrochemical analyzer. Electrochemical impedance spectroscopy experiments were conducted in the frequency range of 0.01–100 kHz with a CHI 600 A electrochemical analyzer.

3 Results and discussion

In the Na-Mn-O system, depending on the sodium contents and reaction temperature, either tunnel compounds (n_{Na}/n_{Mn}<0.45)[10−12] or layered compounds ($0.45 \le n_{Na}/n_{Mn} \le 0.7$)[5, 7−9] can be obtained during synthesis. The XRD patterns of samples with different Na contents are shown in Fig.1. It can be seen from Fig.1 that the content of Na can obviously affect the original structure of sodium manganese oxide. When x is 0.4, a phase of the monoclinic romanechite $Na_{0.4}MnO_2$[12] with tunnel structure is observed. For x=0.5, the sodium manganese oxides with tunnel structure could be mainly obtained and simultaneously accompanied by the formation of layer structure compound. The amount of such layer compound increases by increasing the Na content. For $x \ge 0.6$, it tends to form conventional hexagonal layered P2 structure with space group $P6_3/mmc$[7, 10], in which there are two MO_2 per unit cell and trigonal prismatic sites for Na. For x=1.0, the hexagonal layered structure phase and the impurity phase of $Na_{0.91}MnO_2$[13] are simultaneously observed in the final product.

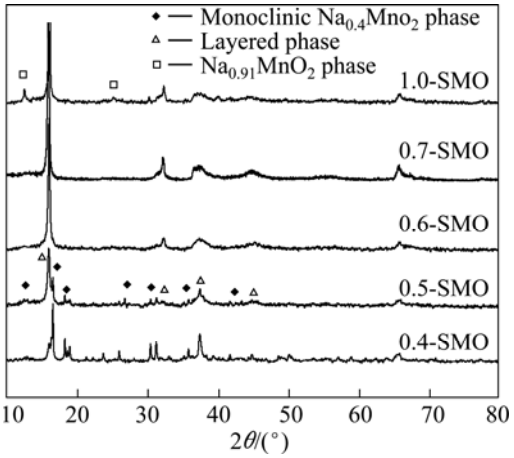

Fig.1 XRD patterns of $Na_xMnO_{2+\delta}$ samples

The SEM photographs for the samples with different Na contents are presented in Fig.2. As can be seen from Fig.2, all these samples are highly porous and consist of an agglomeration of particles with small average grain size. However, 0.6-SMO and 0.7-SMO samples display more homogeneous particle size than 0.4-SMO, 0.5-SMO and 1.0-SMO, implying that 0.6-SMO and 0.7-SMO samples could have better electrochemical performance. The inhomogeneous morphologies of 0.5-SMO and 1.0-SMO samples might be related to the presence of impurity proved by the XRD patterns in Fig.1.

In order to compare the electrochemical performance of the $Na_xMnO_{2+\delta}$ with different sodium contents, the samples were assembled to coin cells. All $Li/Na_xMnO_{2+\delta}$ cells were first discharged and subsequently charged. The initial discharge−charge and the second discharge profiles are shown in Fig. 3. In all samples, a voltage plateau at about 3.0 V during the first discharge is clearly observed. In this process, lithium ions insert into MnO_6 layers and replace parts of sodium ions to become the supporting skeleton of the layer structure[5]. The first charge curves are characterized by two distinct regions, a plateau at about 3.1 V corresponding to the deinsertion of lithium ion and another slight plateau ascribing to initial extraction of sodium ion.

Discharge−charge capacity of $Na_xMnO_{2+\delta}$ with different sodium contents is listed in Table 1. The results reveal that the capacities of the first discharge, first charge and second discharge increase apparently from 0.4-SMO to 0.6-SMO, but decrease from 0.6-SMO to 1.0-SMO. Compared with other samples, the sample 0.6-SMO has the highest charge and discharge capacity: 162 mA·h/g can be intercalated into the cathode in the first discharge process; approximately 207 mA·h/g of Li and Na can be removed during the first charge; 188 mA·h/g of Li corresponding to 0.7 mol Li^+ per unit can insert into MnO_6 layers in the second discharge process.

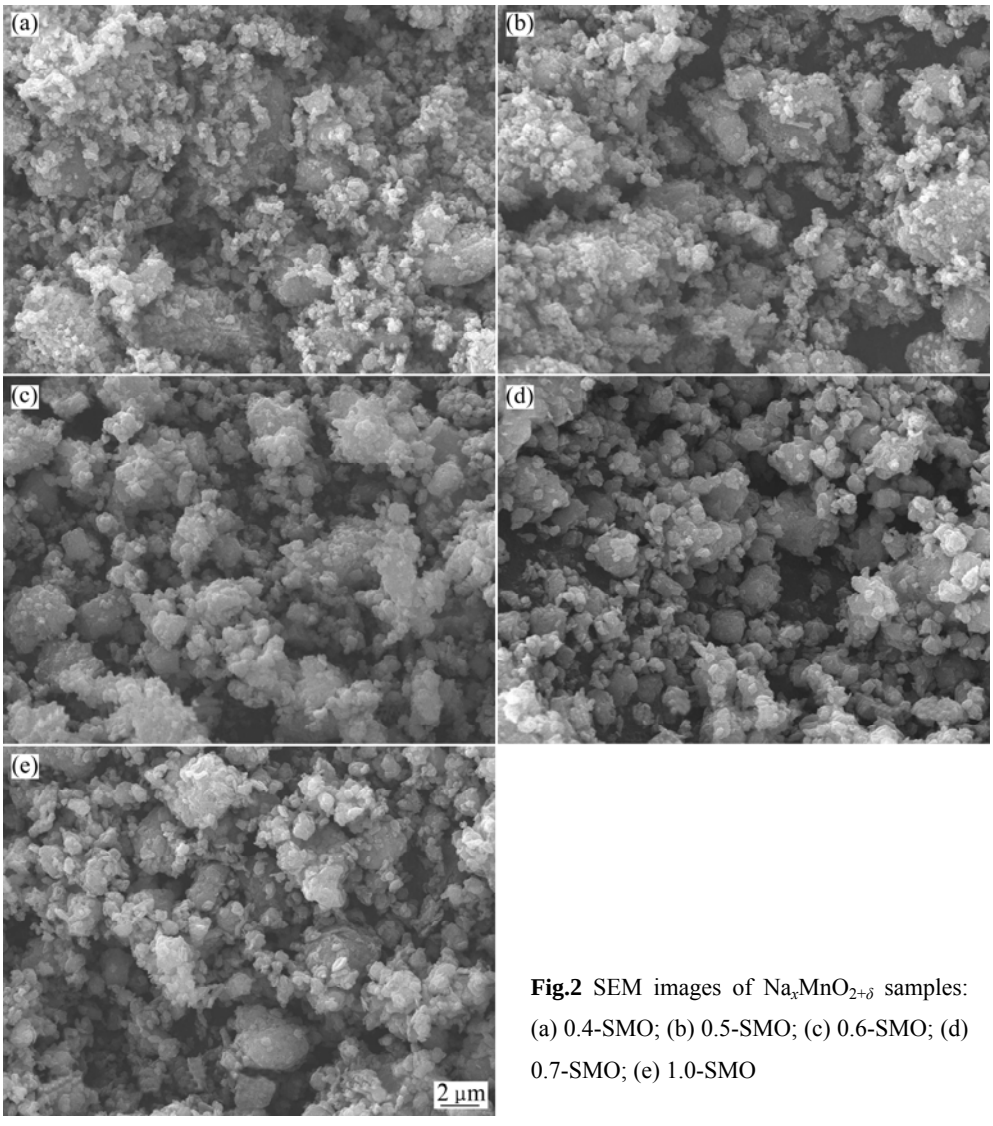

Fig.2 SEM images of $Na_xMnO_{2+\delta}$ samples: (a) 0.4-SMO; (b) 0.5-SMO; (c) 0.6-SMO; (d) 0.7-SMO; (e) 1.0-SMO

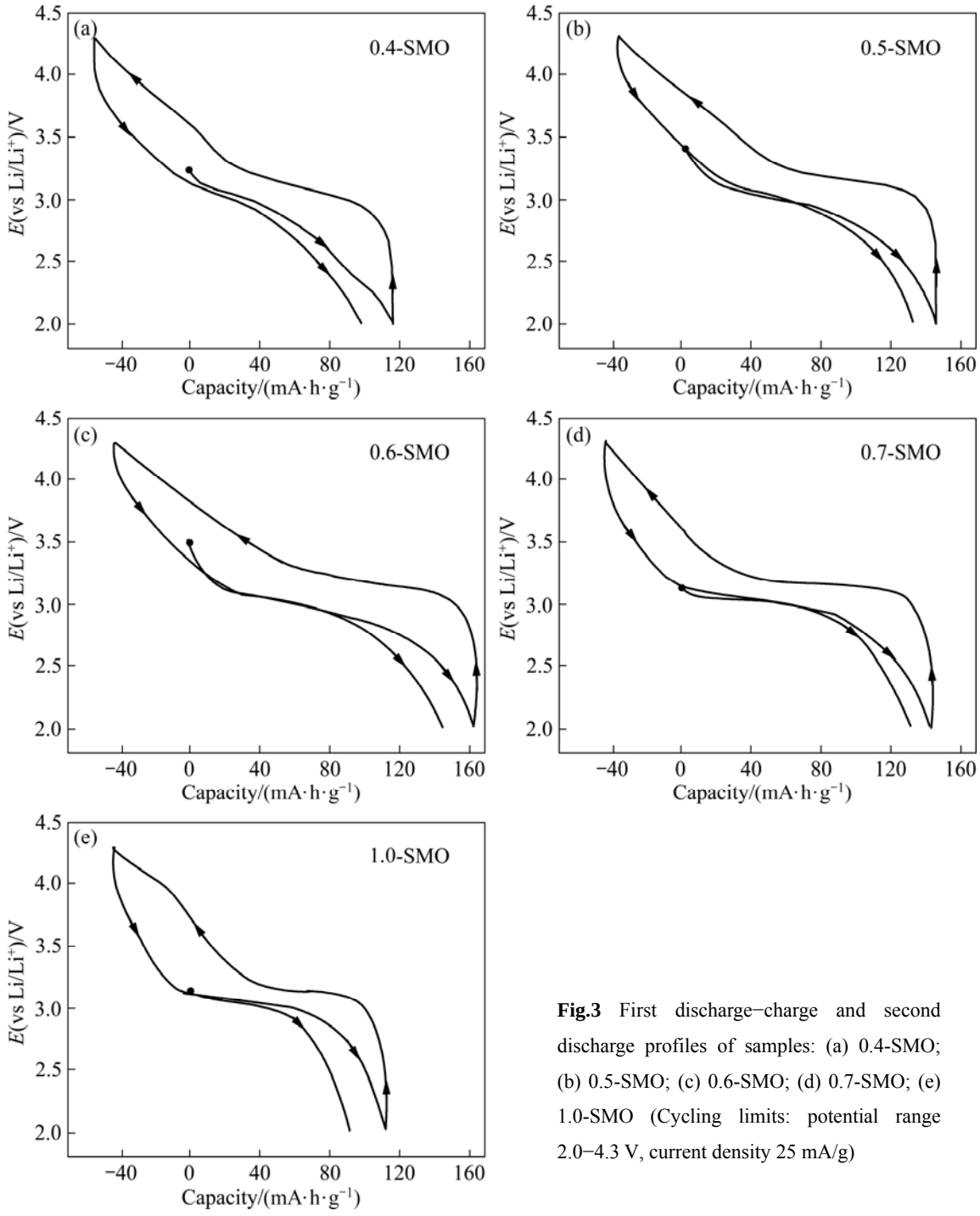

Fig.3 First discharge−charge and second discharge profiles of samples: (a) 0.4-SMO; (b) 0.5-SMO; (c) 0.6-SMO; (d) 0.7-SMO; (e) 1.0-SMO (Cycling limits: potential range 2.0−4.3 V, current density 25 mA/g)

Table 1 Charge−discharge capacity and capacity retention ratio of samples

Sample	First discharge capacity/(mA·h·g^{-1})	First charge capacity/(mA·h·g^{-1})	Second discharge capacity/(mA·h·g^{-1})	30th discharge capacity/(mA·h·g^{-1})	Capacity retention ratio at 30th cycle/%
0.4-SMO	117	172	153	102	66.9
0.5-SMO	146	182	169	137	81.3
0.6-SMO	162	207	188	156	83.0
0.7-SMO	139	187	176	153	86.9
1.0-SMO	112	156	135	119	87.7

Fig.4 shows the cycle performance of samples with different sodium contents, and the charge−discharge capacity and capacity retention ratio of the samples are also listed in Table 1. From the results, it can be concluded that the cyclic stability of $Na_xMnO_{2+\delta}$ with different x values increases with the increase of sodium content. The samples with x = 0.5, 0.6, 0.7 and 1.0 have good cycle performances, and their capacity retention rates are 81.3 %, 83.0 %, 86.9 %, and 87.7 % after 30 cycles, respectively. The sample with x=0.4 has the worst cyclic stability and only 66.9 % of the first discharge capacity is remained after 30 cycles. This is due to monoclinic romanechite $Na_{0.4}MnO_2$ phase that has bad electrochemical performance, which is consistent with results reported by HU and DOEFF[12].

Based on the above-mentioned analysis, it can be found that both 0.6-SMO and 0.7-SMO have stable layer structure and better electrochemical performance. The sample 0.6-SMO delivers the highest second discharge capacity of 188 mA·h/g and retains 77.9 % of its second capacity at the 40th cycle (in Fig.4). As the Na content is increased to 0.7, Li/0.7-SMO cells exhibit the second discharge capacity of 176 mA·h/g and better cyclic stability than 0.6-SMO, and the capacity retention after 40 cycles is close to 85.5 %.

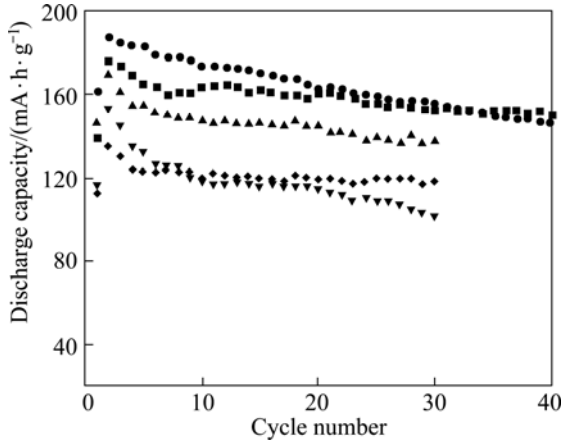

Fig.4 Discharge specific capacity vs cycle number curves for samples (Cycling limits: potential range 2.0−4.3 V, current density 25 mA/g)

Cyclic voltammograms were recorded for the electrodes in the voltage range of 2.0−4.3 V at a scan rate of 50 μV/s after 40 cycles. Voltammograms for the SMO-0.6 and SMO-0.7 samples are shown in Fig.5. For the sample SMO-0.6, two couples of peaks in cathodic sweep and anodic sweep can be seen. It has an anodic peak at 3.41 V with a corresponding cathodic peak at 2.73 V; these peaks are assigned to a Mn^{3+}/Mn^{4+} redox couple[14−15]. Another slightly hump anodic peak at 4.3 V with a corresponding cathodic peak at 3.93 V suggests that the structure transition from layered to spinel-like occurs during the charge−discharge process. This behavior is well consistent with the results that reported by BACH et al[7]. For the sample SMO-0.7, there also are two couples of peaks in cathodic sweep and anodic sweep, but the peak potential differences between the cathodic peak and anodic peak are smaller than those in the SMO-0.6 electrode, indicating that the reversibility of the Li/ 0.7-SMO cell is better than that of Li/ 0.6-SMO cell after 40 cycles. The anodic peak potential and cathodic peak potentials shown in the voltammogram for the samples are basically the same as the charge−discharge cycle curves of the corresponding experiments (see Fig.6).

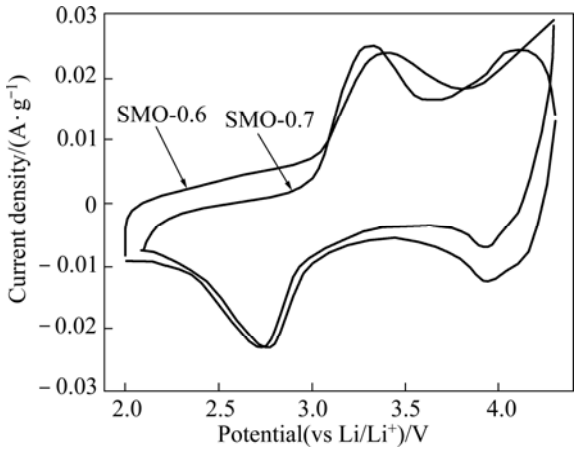

Fig.5 Cyclic voltammograms for samples 0.6-SMO (a) and 0.7-SMO (b) at scan rate of 50 μV/s between 2.0 and 4.3 V

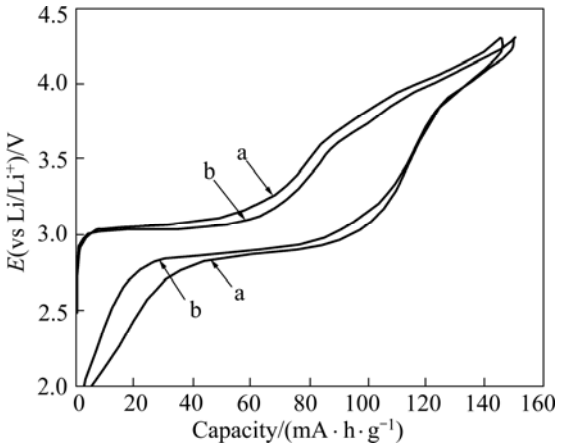

Fig.6 40th cycle discharge−charge profiles of samples 0.6-SMO (a) and 0.7-SMO (b) (Cycling limits: potential range 2.0−4.3 V, and current density 25 mA/g)

In order to further compare these two samples, electrochemical impedance measurements of $Na_{0.6}MnO_{2+\delta}$ and $Na_{0.7}MnO_{2+\delta}$ were performed in the frequency range of 0.01−100 kHz after 40 cycles, and the complex plane impedance plots are shown in Fig.7. The impedance spectrum consists of a depressed arc with a small diameter in the high frequency range and a line

inclined at approximately 60° to the real axis in the low frequency range. The high frequency arc is probably due to the charge transfer reaction and the inclined line in the low frequency range is attributed to Warburg impedance[16]. The latter region corresponds to a frequency range where the kinetics of the system is almost entirely limited by the rate of chemical diffusion process for Li^+ in the host material.

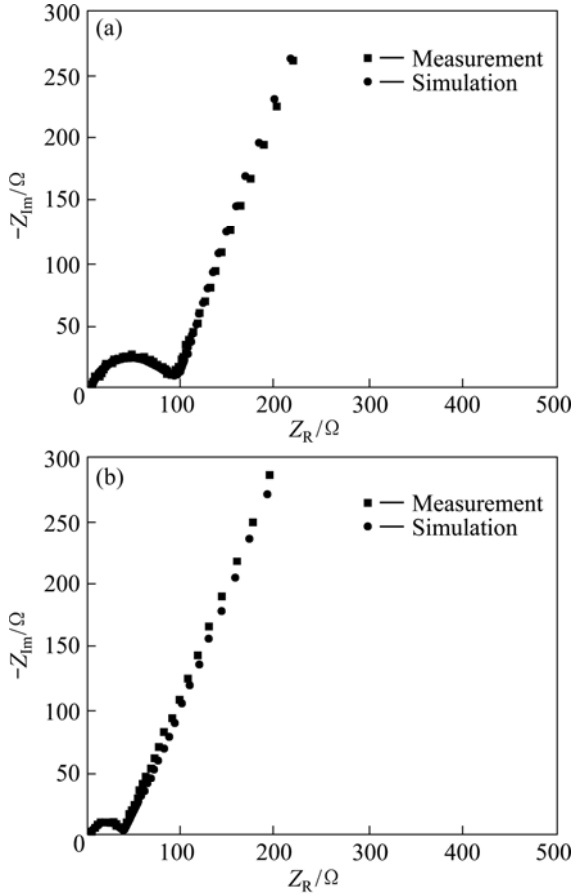

Fig.7 Nyquist plots of samples 0.6-SMO (a) and 0.7-SMO (b)

The equivalent circuit in Fig.8 was used to represent the processes during charge and discharge to assist in analysing the impedance data. R_s, R_{ct}, C and W_o are the ohmic resistance, charge transfer resistance, double layer capacitance and Warburg impedance, respectively. Analysis of the experimental data was performed by fitting equivalent circuits. It can be observed from Fig.7 that the experimental Nyquist diagram is in good agreement with the fitted diagram. Based on the preceding models, every value can be calculated by non-linear least squares, and the results are listed in Table 2. It can be seen from Table 2 that the constant phase angle element (CPE) is defined by two values, CPE_T and CPE_P. The CPE_P values of the samples 0.6-SMO and 0.7-SMO are 0.692 46, 0.723 64, respectively. Both of them approach $\sqrt{3}$, which means that a 60° line is produced on the complex-plane graph. It can be also found that the values of R_{ct} decrease from 87.36 Ω in sample 0.6-SMO to 33.01 Ω in sample 0.7-SMO. This behavior is well consistent with the worse cycle life of the compound 0.6-SMO due to the larger polarization observed in charge−discharge curves[17].

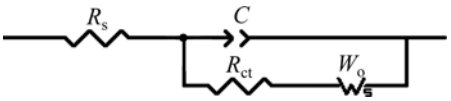

Fig.8 Equivalent circuits for impedance spectra

In order to elucidate the dependence of rate capability of the sample 0.7-SMO, we applied 25, 50, 125 and 250 mA/g for charge and discharge currents across the sodium manganese oxides electrode in the voltage range from 2.0 to 4.3 V. The discharge capacity obtained as a function of the cycle number for different discharge−charge rates (25, 50, 125, 250 mA/g) is shown in Fig.9. During the first ten cycles, the specific discharge capacity fast decreases to 160 mA·h/g (92.5% of the first discharge) at 25 mA/g, then it becomes stable, at last the specific discharge capacity stabilizes at 150 mA·h/g after 30 cycles. The same phenomenon takes place for the cycle life curves at 50 and 125 mA/g. When

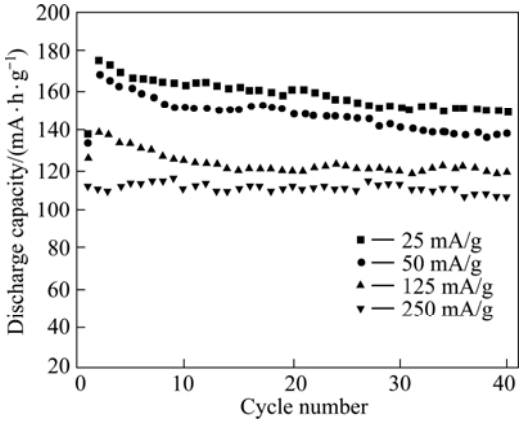

Fig.9 Cycle performances of sample 0.7-SMO under different charge−discharge rates

Table 2 Values of equivalent circuit parameters for 0.6-SMO and 0.7-SMO

Sample	R_s/Ω	$CPE_T/10^{-5}$	CPE_P	R_{ct}/Ω	$W_{o,R}$	$W_{o,T}$	$W_{o,P}$
0.6-SMO	5.427	3.709 3	0.692 46	87.36	2861	50.37	0.711 04
0.7-SMO	4.336	1.825 8	0.723 64	33.01	1721	80.46	0.679 32

CPE_T and CPE_P are two parameters of CPE; $W_{o,R}$, $W_{o,T}$ and $W_{o,P}$ are three parameters of W_o

discharge rate increases to 250 mA/g, the discharge capacity stabilizes at 105 mA·h/g. Overall, the sample 0.7-SMO exhibits good rate capability with discharge capacities of 151 mA·h/g (25 mA/g), 140 mA·h/g (50 mA/g), 120 mA·h/g (125 mA/g) and 112 mA·h/g (250 mA/g) after 40 cycles.

4 Conclusions

1) $Na_xMnO_{2+\delta}$ (x = 0.4, 0.5, 0.6, 0.7, 1.0; δ = 0−0.3) cathode materials with different Na contents were prepared by adjusting the initial stoichiometric ratio of Na to Mn. All these samples are highly porous and consist of an agglomeration of particles with small average grain size. The content of Na can obviously affect the original structure of sodium manganese oxide.

2) The cyclic stability of $Na_xMnO_{2+\delta}$ with different x values increases with the increase of sodium content. The capacities of the first discharge, first charge and second discharge of the samples increase apparently from 0.4-SMO to 0.6-SMO, but decrease from 0.6-SMO to 1.0-SMO. The samples 0.6-SMO and 0.7-SMO have the best electrochemical performance. During discharge−charge cycling, the sample 0.6-SMO gives the highest second discharge capacity of 188 mA·h/g and remains 77.9 % of its second discharge capacity at 25 mA/g after 40 cycles. As x = 0.7, Li/0.7-SMO cells exhibit the second discharge capacity of 176 mA·h/g at 25 mA/g and show better cyclic stability. The capacity retention after 40 cycles is close to 85.5%. Even when discharge current density increases to 250 mA/g, the discharge capacity stabilizes at 105 mA·h/g, indicating that the sample has a stability phase structure and excellent electrochemical performance during cycling process.

3) 0.6-SMO and 0.7-SMO are promising cathode materials for the application in rechargeable lithium cells.

References

[1] TARASCON J M, MCKINNON W R, COOWAR F, BOWMER T N, AMATUCCI G, GUYOMARD D J. Synthesis conditions and oxygen stoichiometry effects on Li insertion into the spinel $LiMn_2O_4$ [J]. J Electrochem Soc, 1994, 141(6): 1421−1431.

[2] GUMMOW R J, DEKOCK A, THACKERAY M M. Improved capacity retention in rechargeable 4 V lithium/lithium-manganese oxide (spinel) cells [J]. Solid State Ion, 1994, 69(1): 59−67.

[3] YANG J S, XU J J. Influence of synthesis conditions on the electrochemical properties of nanostructured amorphous manganese oxide cryogels [J]. J Power Sources, 2003, 122(2): 181−187.

[4] ARMSTRONG A R, PATERSON A, ROBERTSON A J, BRUCE P G. Nonstoichiometric layered $Li_xMn_yO_2$ with a high capacity for lithium intercalation/deintercalation [J]. Chem Mater, 2002, 14(2): 710−719.

[5] GOFF L P, BAFFIER N, BACH S, PEREIRA-RAMOS J P, MESSINA R. Structural and electrochemical characteristics of a lamellar sodium manganese oxide synthesized via a sol-gel process [J]. Solid State Ion, 1993, 61(4): 309−315.

[6] HIBINO M, KAWAOKA H, ZHOU H S, HONAMA I. Rapid discharge performance of composite electrode of hydrated sodium manganese oxide and acetylene black [J]. Electrochim Acta, 2004, 49(28): 5209−5216.

[7] BACH S, PEREIRA-RAMOS J P, WILLMANN P. A sodium layered manganese oxides as 3V cathode materials for secondary lithium batteries [J]. Electrochim Acta, 2006, 52(2): 504−510.

[8] YANG Shui-yi, WANG Xian-you, WEI Jiang-liang, LI Xiu-qin, TANG An-ping. Preparation and electrochemical performance of Na-Mn-O cathode materials [J]. Acta Phys Chim Sin, 2008, 24(9): 1669−1674. (in Chinese)

[9] YANG Shun-yi, WANG Xian-you, WU Wen, HU Tao, WANG Xin, YI Si-yong. Layered $Na_xMnO_{2+\delta}$ as 3V cathode materials for secondary lithium batteries[J]. J Central South University (Science and Technology), 2009, 40(1): 72−77. (in Chinese)

[10] PARANT J P, OLAZCUAGA R, DEVALETTE M, FOUASSIER C, HAGENMULLER P. Sur quelques nouvelles phases de formule Na_xMnO_2 (x≤1) [J]. J Solid State Chem, 1971, 3(1): 1−11.

[11] DOEFF M M, RICHARDSON T J, HOLLINGSWORTH J, YUAN C W, GONZALES M. Synthesis and characterization of a copper-substituted manganese oxide with the $Na_{0.44}MnO_2$ structure [J]. J Power Sources, 2002, 112(1): 294−297.

[12] HU F, DOEFF M M. Electrochemical characterization of manganese oxide cathode materials based on $Na_{0.4}MnO_2$ [J]. J Power Sources, 2004, 129(2): 296−302.

[13] MENDIBOURE A, DELMAS C, HAGENMULLER P. Electrochemical intercalation and deintercalation of Na_xMnO_2 bronzes [J]. Solid State Chem, 1985, 57(3): 323−331.

[14] SUN B, SHEN G P, HU Y L. High-rate capability of spinel $LiNi_{0.05}Mn_{1.95}O_4$ cathode for Li-ion batteries prepared via coprecipitated precursor [J]. Transactions of Nonferrous Metals Society of China, 2007, 17(S1): 937−940.

[15] CHEN Li-bao, HE Yue-hui, TANG Yi-wu. Preparation of ultrafine $LiMn_2O_4$ cathode materials by solid state coordination method [J]. Journal of Central South University (Science and Technology), 2005, 36(3): 390−395. (in Chinese)

[16] WANG X Y, YAN J, YUAN H T, ZHANG Y S, SONG D Y. Impedance studies of nickel hydroxide microencapsulated by cobalt [J]. Int J Hydrogen Energ, 1999, 24: 973−980.

[17] FRANGER S, BACH S, FARCY J, PEREIRA-RAMOUS J P, BAFFIER N. Synthesis, structural and electrochemical characterizations of the sol-gel birnessite $MnO_{1.84}·0.6H_2O$[J]. J Power Sources, 2002, 109(2): 262−275.

(Edited by LI Xiang-qun)